PROCEEDINGS OF SCIENCE

The SENSEI Experiment: sub-GeV dark matter searches with skipper-CCDs

Ana Martina Botti[a,*] **for the SENSEI collaboration**

[a] *Fermi National Accelerator Laboratory, PO Box 500, Batavia IL, 60510, USA*

E-mail: abotti@fnal.gov

Skipper-CCDs are pixeled Silicon-based detectors that can perform multiple non-disruptive measurements of the same charge package. Their sub-electron resolution allows the detection of eV energy transfers, such as that expected from ultra-light dark matter interacting with electrons in a Silicon target. SENSEI (Sub-Electron Noise Skipper Experimental Instrument) is the first experiment to use Skipper-CCD for this purpose and to publish world-leading results using this technology. In this talk, we present an overview of the SENSEI experiment and the current status after the successful commissioning of the second batch of science-grade sensors at SNOLAB. We will also discuss the prospects in rare-events searches with skipper-CCDs: from SENSEI's 100 g detector to OSCURA's 10 kg array, and more.

38th International Cosmic Ray Conference (ICRC2023)
26 July - 3 August, 2023
Nagoya, Japan

*Speaker

PoS(ICRC2023)1398

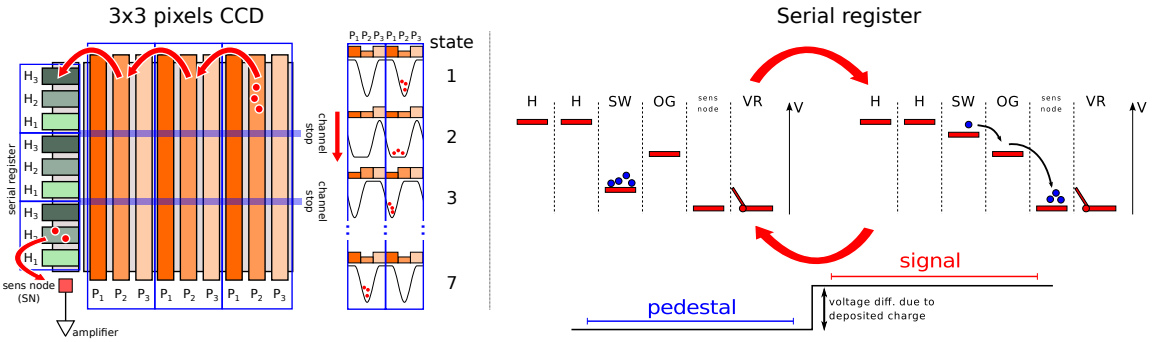

Figure 1: (Left) schematic of the process to transport collected charges to the output stage. (Right) representation of the Skipper-CCD read-out.

1. The SENSEI Experiment

SENSEI (Sub-Electron-Noise Skipper-CCD Experimental Instrument) is the first experiment to implement skipper-CCDs for dark-matter detection. Skipper-CCDs are charge-coupled devices [1] with a floating gate [2, 3] at the output stage, which allows for multiple lectures of the collected charges in a non-disruptive way. This boosted the capabilities of scientific high-resistivity fully-depleted CCDs [4] by reducing their read-out noise; achieving sub-electron resolution [5] enhanced the CCD technology to detect interactions in Silicon where only a few hole-electron pairs are produced, as well as to obtain precise measurements of silicon properties using X-ray interactions with larger energy transfers [6–9].

When a particle impinges on the silicon crystal, it produces electron-hole pairs by transferring energy to the lattice. Regardless of the process by which the electron-hole pairs are produced, once electrons jump to the conduction band they are accelerated towards the CCD surface by applying a bias voltage between the CCD terminals. At the surface, we transport the charges towards the output stage, dubbed serial register, as we illustrate in the left panel of Fig 1 where we present an example of a 3×3-pixel CCD. Using a series of vertical clocks to set potential wells along the pixels, we can move the charge through the vertical tracks. We show the time representation of this process as states one to seven in Fig 1. After reaching the serial register, the charge is transported towards a floating gate, dubbed sense node, with a series of horizontal clocks as before. These devices have a high transport efficiency, which is necessary to accurately reconstruct the energy deposit in the silicon bulk.

In the right panel of Fig. 1, we present a schematic of the serial register for a Skipper-CCD. We use the horizontal clocks to move the charge towards the summing well gate and then to the sense node through the output gate [10]. The novelty in the skipper technology is that by implementing a floating gate, we can read the charge in a non-disruptive way and move it back and forward from the sense node to the summing well to obtain multiple measurements of the same charge. Each measurement consists of first integrating the signal in a certain time window when the sense node is empty (left in the schematics) to obtain the signal baseline or pedestal. Then, we move the charges into the sense node (right in the schematics) and repeat the integration to extract the signal. By subtracting the signal and pedestal we obtain a voltage relative to the number of collected charges. This correlated double sampling technique [11] is appropriate to subtract the high-frequency noise

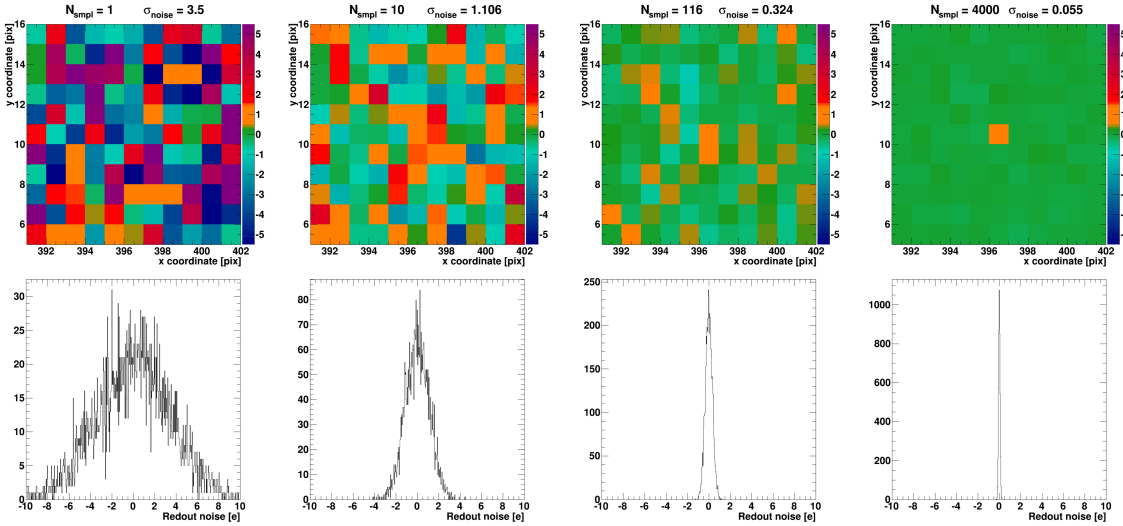

Figure 2: (Top) images obtained with a Skipper-CCD using 1, 10, 116, and 4000 samples. (Bottom) charge distribution of the pixels in the images on the top.

since it is averaged to zero at each integration, and the remaining offset is then subtracted. However, it is not enough to remove the noise when $\frac{1}{f}$ is larger than the integration window, where f is the noise frequency.

The low-frequency noise is the main contribution to the detector energy resolution; this is a few electrons for traditional CCDs. With Skipper-CCDs, we improved this scenario since using the floating gate to perform several measurements of the output charge allows us to achieve sub-electron noise. If for each sample the noise is uncorrelated and roughly Gaussian, the total read-out noise after averaging all the samples is $\sigma_N = \frac{\sigma_1}{\sqrt{N}}$, where σ_1 is the noise for one sample and N the number of samples. To illustrate this, we present in the top panels of Fig. 2 cropped images consisting of mainly empty pixels obtained with a skipper-CCD using 1, 10, 116, and 4000 samples. In the bottom panels of Fig. 2 we present the charge distribution in the number of electrons for each image.

After performing multiple samples and achieving sub-electron noise, Skipper-CCDs behave as low-energy calorimeters with an energy bin almost as low as the mean pair creation energy in Silicon (about 3.7 eV [7]). In this sense, these devices have unprecedented sensitivity to detect sub-GeV dark-matter particles that may produce electron recoils through scattering or absorption [12] since the expected rate of these interactions decreases about 1 order magnitude every time the detector threshold increases in one or two electrons.

In this work, we present results from two science run using skipper-CCDs. The first consists of a reanalysis of data obtained at the shallow underground facility at Fermilab, MINOS [13]. The second consist of the first science run of SENSEI at a deep underground facility, SNOLAB.

2. The MINOS setup

The MINOS underground hall at Fermilab was strategically chosen due to its capability (230 m.w.e) to shield the detector from air shower muons and its historical usage for testing sensitive particle detector technology. The SENSEI setup, positioned 1 km away from the NuMI beam

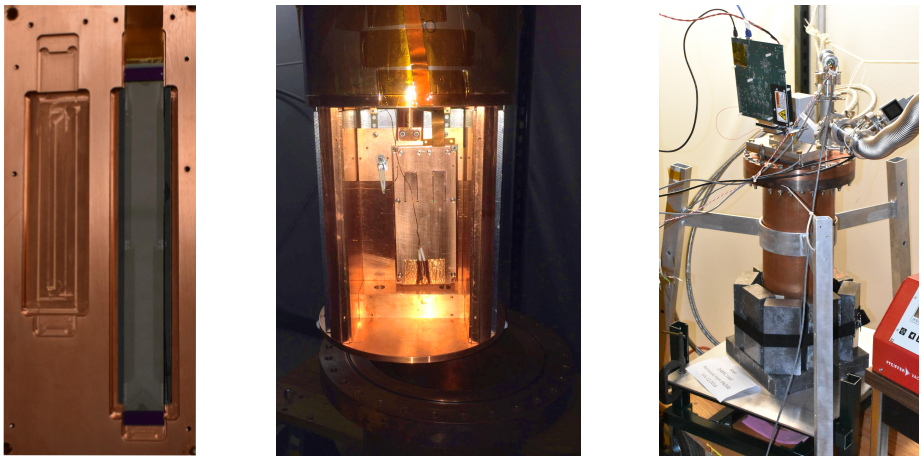

Figure 3: (Left) Skipper-CCD deployed in a copper tray; where a copper leaf-spring maintains constant pressure for consistent thermal contact. (Middle) Picture of the open shield with the Skipper-CCD module. (Right) Picture of the closed setup with a 3-inch lead block shield over the sensor.

target, was primarily aimed at searching for sub-GeV dark matter originating from astrophysical sources [13]. However, the data obtained during the periods where the NuMI beam was on also allowed us to set constraints on milli-charged particles (mCPs) production at the NuMI beam [14]. We used a Skipper-CCD designed at LBNL consisting of 1.926 g of high-resistivity silicon (about 18 kΩcm) with an active area of $9.216 \times 1.329\,\mathrm{cm}^2$, 675 μm thickness, and 5443584 pixels. We show a picture of the device deployed in a cold copper box for shielding infrared photons on the left panel of Fig.3. We connect the CCD to a flex cable using an aluminum circuit printed on a silicon substrate, and the flex cable to a low-threshold acquisition board (LTA) [15]. The module was situated in the same vessel used for a previous run [16] and an additional lead shielding was deployed around the vessel to reduce the high-energy backgrounds (see middle and right panels in Fig. 3). We operated the CCD at 135 K with the support of a cryocooler, a PID temperature controller, and a vacuum pump to maintain a pressure below 2×10^{-4} mbar. The CCD was biased at 70 V, and we obtained 22 blinded images with a 20-hours exposure and 5.153-hour readout time using four amplifiers each to read one quadrant of the CCD. For each pixel, we obtained 300 samples at a read-out speed of 42.825μs, with a resulting noise of $0.14\,\mathrm{e}^-$.

3. The SNOLAB setup

The full SENSEI experiment is being deployed at SNOLAB: a deep underground facility with 6000 m.w.e. The first science run was performed between September 2022, and April 2023 using 6 skipper-CCDs designed at LBNL with 2.23 g of high-resistivity silicon. Each consisted of 6144×1024 pixels of $15 \times 15\mu\mathrm{m}^2$ and 675μm thickness. We show a picture of the package in the top-left panel in Fig. 4. We glue the CCD to a silicon substrate for thermal conductivity and connect the CCD pads to a flex cable that goes into the read-out electronics (LTA board [15]). We installed the CCDs in pairs inside a cold copper tray, and deploy these inside a cold copper box (top-middle-left panel in Fig. 4). Then, we installed 6-in copper bricks and a hat around the sensors, as presented in the top-middle-tight panel in Fig. 4. We show the whole closed vessel installed on

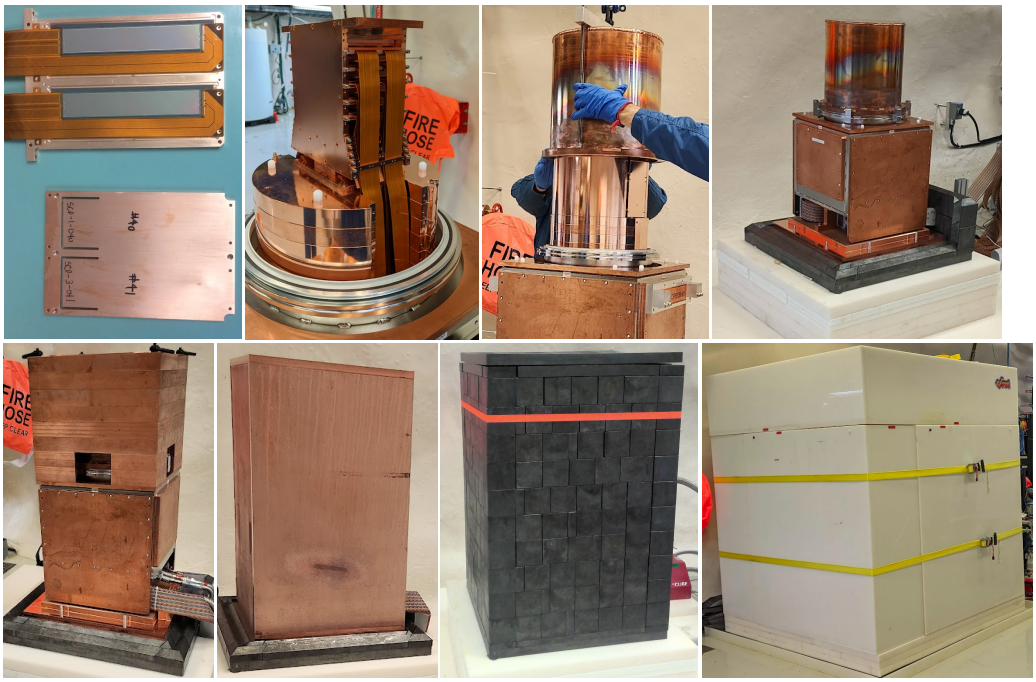

Figure 4: SENSEI setup at SNOLAB. (Top-left) two CCDs deployed in the copper box. (Top-middle-left) cold copper box deployed inside the vessel (Top-middle-right) Closing of the copper hat after deploying inner shield bricks (Top-right) The SENSEI vessel after closing (Bottom-left) first outer copper shield (Bottom-middle-left) second copper shield (Bottom-middle-right) lead shield (Bottom-right) polyethylene and water shield

the platforms for the outer shields in the top-left panel in Fig. 4. In the bottom panels of Fig 4. we present the copper shields for electrons and x-rays (left and middle left), the 3-inch lead gamma-ray shield (middle right), and the neutron 42-inch polyethylene and water shield (right).

We cool down the CCDs through a cold finger at a temperature range between 125 and 145 K. Each CCD was biased with 70 V, and we collected 300 samples per pixel, with a single-sample readout noise of 2.4 e^- and time of 48.8 μs. We obtained a 20-hour exposure, and a total readout time of 7.69 hours, using four amplifiers each to read one quadrant of the CCD. We obtained 129 images (70 commissioning and 59 blinded).

4. Analysis and quality cuts

The first step towards the data selection consists of a series of masks, each targeting a particular background source. The masks remove specific pixels from each image according to the spatial correlation with the clusters; we then remove all masked pixels from the subsequent analysis. These masks were developed using the commissioning dataset and were then implemented into the commissioning and blinded datasets for the final analysis. Even though the masking for the MINOS and SNOLAB data are different (since the backgrounds are different), the dominant cuts are similar. In Fig 5, we present two sections of MINOS (left) and SNOLAB (right) data. The difference in occupancy is apparent due to the thicker shield and overburden of SNOLAB. We also present in colors the results after masking the images; only the pixels in black are used in the dark

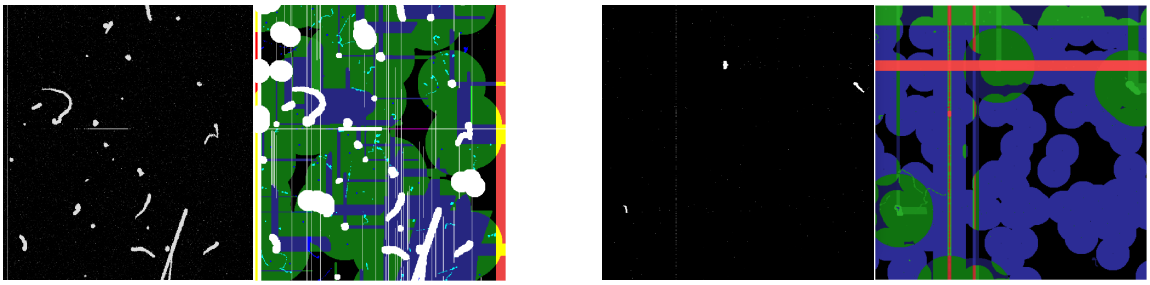

Figure 5: Example of (Left) MINOS and (Right) SNOLAB data. In colors, we present the masking of the images.

matter analysis. Some of the most significant masks are the halo mask (green circles), designed to remove the Cherenkov radiation produced by high energy charged particles, the bleeding zone mask (blue lines), designed to remove the electrons that are left behind when transferring the high-energy events to the read-out stage, and the low-energy cluster mask, only for SNOLAB data (blue circles), aimed at removing the disjoint groupings of charge that are indicative of nonuniform generation in the detector. The lower occupancy in the SNOLAB data, allowed us to develop higher-quality masks while conserving statistics for the analysis.

For the MINOS data, we discuss the details of the analysis in [13], and we extended it to clusters with 5 and 6 e^- to obtain the results presented in this work. For the SNOLAB data, we excluded quadrants with high densities of single electron events after applying quality cuts or high readout noise during the commissioning phase. The quadrants tagged as "good" had a readout noise of 0.14 e^- and single-electron event densities of approximately 2×10^{-4} e^-/pixel. Additionally, we removed images collected during periods of higher temperature exhibited correspondingly higher densities of single-electron events. Following this selection process, a total of 82 good images (45 from the commissioning phase and 37 from the blinded phase) remained, resulting in a cumulative exposure of 542.90 g-days (297.93 g-days from commissioning and 244.97 g-days from blinded data) before any additional cuts were applied. After applying the necessary masks, we obtained a total exposure of about 70 g-days.

5. Latest results

For mCP interacting with the MINOS detector, the likelihood of an electron recoil ionizing 1-6 e^- in the silicon, which corresponds to (~1.2–20 eV) energy depositions, is determined by the model outlined in [18]. The cross-section calculation and the convolution with the probability of producing electron-hole pairs for each individual channel are demonstrated in [14]. In the left panel of Fig. 6, we show the 95% C.L. constraints on the mCP parameter space from the published SENSEI data at MINOS, and compared it with the existing bounds from other experiments. This limit was calculated for each electron channel independently, taking into account their different backgrounds, and then combined using a frequentist approach based on the likelihood ratio as in [13].

To constrain dark matter that scatters off electrons [12] with the SNOLAB data, we calculated the dark-matter-electron scattering cross-section with *QEDark* [19] using the dark-matter halo

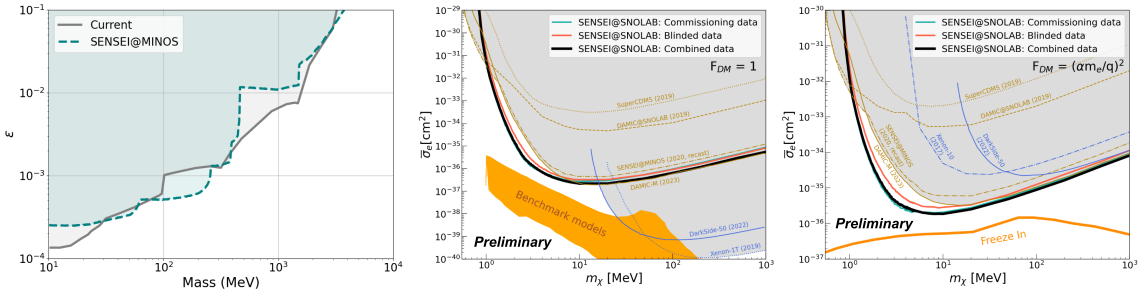

Figure 6: (Left) Cyan line/region shows the 95% C.L. limit on mCPs from the SENSEI data collected in the MINOS cavern in 2020. Gray line/region shows constraints from other experiments [14]. (Middle) DM-electron scattering for a heavy mediator, $F_{\rm DM} = 1$ and (Right) light mediator, $F_{\rm DM} \propto 1/q^2$. The new SENSEI@SNOLAB limits are shown in black for the combined data, red for the blinded data, and cyan for the commissioning data. Current constraints are shown in the gray-shaded region, where the noble liquid experiments are given in blue while solid-state detectors are shown in gold. Interesting theoretical targets are shown in orange.

parameters recommended in [20]. We follow [18] to compute the number of electrons produced by an interaction that transfers energy to an electron within the CCD; this model includes Fano-like fluctuations. In Fig. 6, we show the resulting 90% C.L. limit for dark matter scattering with electrons in a Silicon target through a light (middle panel) and heavy (right panel) mediator. We used a likelihood-ratio test based on [21], with a toy montecarlo (instead of the asymptotic approximation) to compute the distribution of the statistics used for the calculation of the p-value.

6. Summary and outlook

In the last years, we proved that Skipper-CCDs are a promising technology for rare events and new physics searches where sensitivity to low-energy transfer processes is required. SENSEI is the first experiment using this technology for this purpose and the first to produce world-leading results. In this work, we reported a new leading limit for mCP production in beams at the mass region of 100 to 210 MeV using the first run with a science-grade skipper-CCD at MINOS. Furthermore, we presented results for the first SENSEI science run in SNOLAB, which produced leading limits in the 1-10 MeV and 1-1000 MeV mass regions for dark matter-electron scatterings through heavy and light mediators.

SENSEI will start a new science run this year at SNOLAB, with 19 skipper-CCDs, more than three times the mass used for this work; in the future, we intend to achieve a total active mass of 100 g. In addition, DAMIC(-M) is currently upgrading to skipper-CCDs aiming at a total active mass of 1 kg in the next three years [22], followed by the Observatory of Skipper CCDs Unveiling Recoiling Atoms (OSCURA) project, which foresees a Skipper-CCD detector with a total mass of 10 kg on 2027 [23].

We show the expectations for the SENSEI final design (solid cyan line), DAMIC-M (solid red line), and OSCURA (solid blue line) in Fig. 7 for dark matter interacting through a light (left) and heavy (middle) mediator, assuming a zero background for channels with two or more electrons.

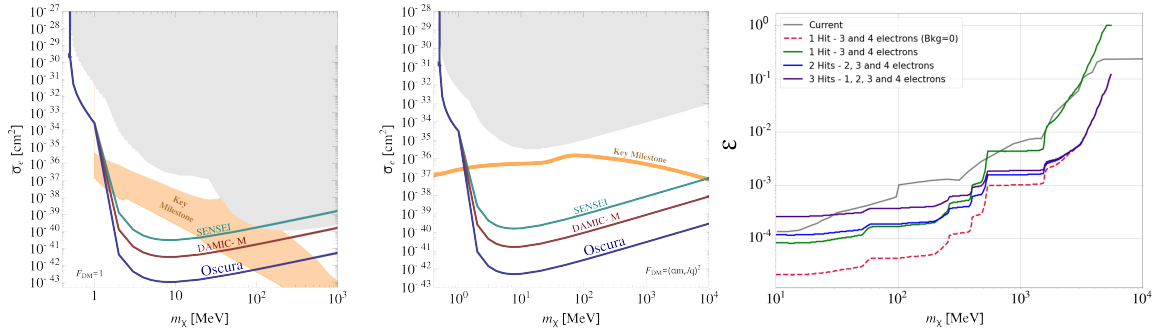

Figure 7: Projected sensitivities for SENSEI, DAMIC-M and OSCURA for a heavy (left) and light (middle) mediator. Other experiment results are shown in gray shade. Figure adapted from [24]. (Right) Projected constraints for mCPs with a 90% C.L for a 1 kg skipper-CCD detector at the NuMI beamline [25].

Previous results are shown in a gray shade. In orange, we present the theoretical milestone scenarios, which will be explored with the next generation of Skipper-CCD detectors.

Finally, similar to the search for mCP at MINOS, we computed the projections for having a skipper-CCD detector to hunt mCP particles at the NuMI beam line and presented on the right panel of Fig. 7. We assume 1 kg of active mass and 2 $\times 10^{18}$ POT beam. We computed the projections using different track geometries [25]. The gray line denotes the current limits set by other experiments.

References

[1] G. E. Smith. Rev. Mod. Phys. **82** (2010) 2307-2312.
[2] J. R. Janesick, et al. , SPIE **1242** (1990) 223-237.
[3] D. Wen, IEEE J. Solid-State Circuits **6** (1974) 410.
[4] S. Holland et al., IEEE Transactions on Electron Devices **50** (2003) 223-238.
[5] J. Tiffenberg, Phys. Rev. Lett. **119** (2017) 6.
[6] D. Rodrigues et al., Nucl. Instrum. Meth. A **1010** (2021) 165511.
[7] D. Rodrigues et al., arXiv:2305.09005 (2023).
[8] A. M. Botti et al., Phys. Rev. D **106** (2022) 072005.
[9] D. Norcini et al., Phys. Rev. D **106** (2022) 092001.
[10] G. Fernandez-Moroni et al., Exp. Astron. **34** (2012) 43-64.
[11] M. H. White, et al.,IEEE J. Solid-State Circuits **9** (1974) 1-12.
[12] R. Essig et al., J. High Energy Phys **05** (2016) 046.
[13] The SENSEI collaboration. Phys. Rev. Lett. **125** (2020) 171802.
[14] The SENSEI Collaboration., arXiv:2305.04964 (2023)
[15] g. Cancelo et al., J.Astron.Telesc.Instrum.Syst. **7** (2021) 015001.
[16] The SENSEI collaboration. Phys. Rev. Lett. **122** (2019) 161801.
[17] QEDark, https://github.com/tientienyu/QEdark
[18] K. Ramanathan, N. Kurinsky, Phys. Rev. D **102** (2020) 063026
[19] QEDark, https://github.com/tientienyu/QEdark
[20] D. Baxter et al., Eur. Phys. J. C **81** (2021) 907
[21] G. Cowan et al., Eur. Phys. J. C **71** (2021) 1554
[22] The DAMIC collaboration. Nucl. Instrum. Meth. A **958** (2020) 162933.
[23] A. Aguilar-Arevalo et al., arXiv:2202.10518 (2022)
[24] B. Cervantes et al., arXiv:2304.04401 (2023)
[25] S.Perez et al., arXiv:2304.08625 (2023)